

PbO / PbF₂ Flux Growth of YScO₃ and LaScO₃ Single Crystals – Structure and Solid-State NMR Spectroscopy

Sarkarainadar Balamurugan^a, Ute Ch. Rodewald^a, Thomas Harmening^a, Leo van Wüllen^b, Daniel Mohr^b, Heinz Deters^b, Hellmut Eckert^b, and Rainer Pöttgen^a

^a Institut für Anorganische und Analytische Chemie and NRW Graduate School of Chemistry, Universität Münster, Corrensstraße 30, 48149 Münster, Germany

^b Institut für Physikalische Chemie and NRW Graduate School of Chemistry, Corrensstraße 30, Universität Münster, 48149 Münster, Germany

Reprint requests to R. Pöttgen. E-mail: pottgen@uni-muenster.de

Z. Naturforsch. 2010, 65b, 1199 – 1205; received May 14, 2010

Well-shaped small single crystals of the orthorhombic perovskites YScO₃ and LaScO₃ were grown from mixtures of the corresponding sesquioxides RE₂O₃ in PbO/PbF₂ fluxes. Both structures were refined from single-crystal diffractometer data: GdFeO₃-type, *Pnma*, $a = 570.68(7)$, $b = 789.3(1)$, $c = 542.44(7)$ pm, $wR2 = 0.0363$, 448 F^2 values for Y_{0.96}ScO_{2.94}, and $a = 579.68(9)$, $b = 810.3(2)$, $c = 568.3(1)$ pm, $wR2 = 0.0387$, 513 F^2 values for La_{0.94}ScO_{2.91}, with 32 variables per refinement. The 4c rare-earth sites of both perovskites show small defects which are charge-compensated by defects on both oxygen sites, leading to the compositions La_{0.94}ScO_{2.91} and Y_{0.96}ScO_{2.94} for the investigated crystals. The rare-earth sites have been characterized by ⁸⁹Y and ⁴⁵Sc magic-angle spinning (MAS) NMR. The ⁴⁵Sc quadrupolar interaction parameters extracted from these spectra by simulations are found to be in good agreement with those obtained from DFT calculations of the electric field gradient.

Key words: Scandium, Crystal Chemistry, Solid-State NMR

Introduction

The sesquioxides of the rare earth (RE) elements have widely been studied with respect to their structural (polymorphism) and thermodynamic behavior as well as their interesting physical properties. They are host materials for RE³⁺ luminescence and for dielectrics for high- κ applications as bulk and thin film materials, and they have been used for ion-sensitive field-effect transistors. Overviews on these topics are given in several review articles [1, 2, and refs. therein]. Depending on the size of the RE³⁺ cation, temperature and pressure, the RE₂O₃ sesquioxides crystallize with different structure types, called the A-, B- and C-type. Also a variety of mixed rare earth phases RERE'O₃ have been investigated. If the two rare earth cations are sufficiently different in size, full ordering of the cations on distinct crystallographic sites takes place. This is especially possible if the smallest rare earth cation Sc³⁺ is used. Such compounds crystallize with the orthorhombic GdFeO₃-type structure [3], space group *Pnma*.

In the course of our systematic studies on ⁴⁵Sc solid-state NMR parameters [4–7, and refs. therein], we were interested in the diamagnetic RERE'O₃ oxides YScO₃ and LaScO₃. The largest difference in the ionic radii occurs for LaScO₃ which adopts the GdFeO₃-type over the whole temperature range [8, 9]. YScO₃ shows a cubic, bixbyite-type high-temperature [10, 11] modification with random cation distribution (similar to binary Sc₂O₃ [12]) and an ordered GdFeO₃-type low-temperature [8, 13] modification. For LuScO₃ only the cubic, disordered form has been observed [14]. The course of these ordering phenomena corresponds with the course of the difference in the ionic radii of the RE³⁺ cations. GdFeO₃-type LuScO₃ can only be obtained in the form of metastable thin films [15].

⁴⁵Sc solid-state NMR has so far only been applied to few intermetallic and oxidic systems [4–7, 16–25, and refs. therein]. In these references ⁴⁵Sc NMR has effectively been used for the differentiation of different atomic sites and vacancy formation. In extension of our work on intermetallic scandium compounds we have

now investigated YScO₃ and LaScO₃ in order to further complete the data base for ⁴⁵Sc solid-state NMR parameters.

Experimental Section

Syntheses

Chemical ingredients used for the syntheses of LnScO₃ (Ln = Y and La) were Y₂O₃ (Chempur, > 99.9%), La₂O₃ (Chempur, > 99.9%), Yb₂O₃ (Chempur, > 99.9%), Sc₂O₃ (Acros Organics, 99.9%), PbO (ABCR, 99.5%), and PbF₂ (ABCR, > 99.5%). Appropriate amounts of Ln₂O₃ and Sc₂O₃ were thoroughly mixed and ground in an agate mortar with pestle under acetone and ethanol in order to obtain homogeneous starting mixtures for the synthesis of the desired compounds. PbF₂ and PbO were used as flux reagents. This technique was originally used by Remeika for the growth of rare earth orthoferrite crystals [26].

Single crystals of LnScO₃ (Ln = Y and La) were grown from mixtures of the sesquioxides with the flux reagents PbF₂ and PbO in molar ratios 1 : 6 : 6 and 1 : 6 : 12 for Y and La, respectively. These reaction mixtures were transformed into small pellets at 2 tons applied pressure. One of these pellets was placed in a platinum crucible covered with a platinum lid, and the crucible was then placed in a square shaped high-purity alumina crucible in order to avoid direct contact with the furnace. For the synthesis of YScO₃, the crucible was heated to 1423 K within 1 h, and the temperature was maintained for 12 h in the muffle furnace (Carbolite RHF 1500). After that the temperature was slowly decreased to 873 K at a cooling rate of 25 K h⁻¹, and then to r. t. with a rate of 100 K h⁻¹. In the case of LaScO₃, the crucible was inserted into the preheated furnace at 1073 K, heated to 1573 K at a rate of 100 K h⁻¹, and held for 12 h in the furnace. After that the temperature was decreased to 1073 K at a rate of 200 K h⁻¹ and the container then finally quenched to r. t. by pulling it out from the furnace. The reaction products consisted of small crystals. They were isolated from the reaction products through extraction of the (remaining) flux with hot dilute hydrochloric acid.

For ⁴⁵Sc NMR measurements, good quality polycrystalline samples were prepared from appropriate reaction mixtures kept at 1573–1873 K for 150 h with three intermediate regrinding steps in alumina crucibles. For the ⁸⁹Y NMR data collection quite similar preparation conditions were employed for the synthesis of a doped YScO₃ : Yb 1% polycrystalline sample.

EDX analyses

The single crystals measured on the diffractometer were analyzed by energy dispersive analyses of X-rays using a Leica 420i scanning electron microscope attached to an EDX (Energy Dispersive Analysis of X-Rays) unit. The crystal

Table 1. Crystal data and structure refinement for LnScO₃; Ln = Y and La; GdFeO₃-type, space group *Pnma*, Z = 4.

Empirical formula	Y _{0.96} ScO _{2.94}	La _{0.94} ScO _{2.91}
Molar mass, g mol ⁻¹	177.88	221.36
Lattice parameters (Guinier powder data)		
<i>a</i> , pm	570.68(7)	579.68(9)
<i>b</i> , pm	789.3(1)	810.3(2)
<i>c</i> , pm	542.44(7)	568.3(1)
Cell volume, nm ³	<i>V</i> = 0.2443	<i>V</i> = 0.2669
Calculated density, g cm ⁻³	4.84	5.51
Crystal size, μm ³	40 × 40 × 100	40 × 40 × 60
Transmission (max/min)	1.58	1.46
Abs. coefficient, mm ⁻¹	25.3	17.1
Exposure time, min	4	3
Detector distance, mm	80	80
ω range; increment, deg	0–180; 1.0	0–180; 1.0
Integr. Parameter A, B, EMS	14.0; 4.0; 0.022	14.0; 4.0; 0.020
<i>F</i> (000), e	329	390
θ range, deg	4–32	4–33
Range in <i>hkl</i>	±8, ±11, ±8	±8, ±12, ±8
Total no. reflections	3784	6986
Independent reflections	448	513
Reflections with <i>I</i> ≥ 2σ(<i>I</i>)	400	434
Data / parameters	448 / 32	513 / 32
<i>R</i> 1/ <i>wR</i> 2 for <i>I</i> ≥ 2σ(<i>I</i>)	0.0157 / 0.0357	0.0178 / 0.0373
<i>R</i> 1/ <i>wR</i> 2 for all data	0.0195 / 0.0363	0.0250 / 0.0387
Goodness-of-fit on <i>F</i> ²	0.992	0.981
Extinction coefficient	0.043(2)	0.0067(6)
Largest diff. peak / hole, e Å ⁻³	0.60 / -0.79	1.27 / -1.44

mounted on a quartz fiber was first coated with a thin carbon film to ensure conductivity. The semi-quantitative analyses with LaF₃, YF₃, Sc, and SiO₂ as standards were in good agreement with the proposed metal composition. No impurity elements were detected. Special care was taken in detecting a possible fluorine content originating from the PbF₂-containing flux.

X-Ray powder diffraction

The phase purity and structure of the synthesized samples were characterized by X-ray powder diffraction through Guinier powder patterns using CuK α ₁ radiation (λ = 154.056 pm) and α -quartz (*a* = 491.30 pm, *c* = 540.46 pm) as an internal standard. The Guinier camera was equipped with an imaging plate system (Fujifilm, BAS-Reader 1800). The orthorhombic lattice parameters (Table 1) were obtained from least-squares fits of the powder data. The correct indexing of the patterns was ensured by intensity calculations [27]. Our experimental data are in good agreement with the literature data [8, 9, 13].

Single-crystal X-ray diffraction

Well-shaped single crystals were selected from the samples prepared in the PbO / PbF₂ flux. They were first examined by Laue photographs with white Mo radiation on a Buerger precession camera (equipped with an image plate

Atom	Wyck.	Occup.	<i>x</i>	<i>y</i>	<i>z</i>	<i>U</i> _{eq}
Y_{0.96}ScO_{2.94}						
Y	4 <i>c</i>	0.964(1)	0.06192(4)	1/4	0.01751(4)	40(1)
Sc	4 <i>b</i>	1.0	0	0	1/2	29(1)
O1	4 <i>c</i>	0.984(7)	0.4431(4)	1/4	0.8725(3)	59(4)
O2	8 <i>d</i>	0.981(4)	0.1930(3)	0.9342(2)	0.8103(2)	76(3)
La_{0.94}ScO_{2.91}						
La	4 <i>c</i>	0.936(1)	0.04217(4)	1/4	0.01004(4)	47(1)
Sc	4 <i>b</i>	1.0	0	0	1/2	26(1)
O1	4 <i>c</i>	0.948(12)	0.4684(6)	1/4	0.9054(5)	73(8)
O2	8 <i>d</i>	0.978(6)	0.2042(4)	0.9496(3)	0.7957(4)	100(5)

Table 2. Atomic coordinates and isotropic displacement parameters (pm²) of LnScO₃; Ln = Y and La. *U*_{eq} is defined as one third of the trace of the orthogonalized *U*_{ij} tensor.

Table 3. Anisotropic displacement parameters (pm²) of Y_{0.96}ScO_{2.94} and La_{0.94}ScO_{2.91}.

Atom	<i>U</i> ₁₁	<i>U</i> ₂₂	<i>U</i> ₃₃	<i>U</i> ₁₂	<i>U</i> ₁₃	<i>U</i> ₂₃
Y_{0.96}ScO_{2.94}						
Y	28(1)	57(1)	36(1)	0	6(1)	0
Sc	23(2)	35(2)	30(2)	5(1)	1(1)	4(1)
O1	56(9)	46(8)	75(8)	0	-1(6)	0
O2	59(6)	100(6)	68(5)	-22(5)	-24(4)	16(4)
La_{0.94}ScO_{2.91}						
La	56(1)	44(1)	42(1)	0	10(1)	0
Sc	23(3)	23(3)	31(3)	3(2)	1(2)	1(2)
O1	110(16)	27(14)	83(12)	0	1(11)	0
O2	102(10)	120(11)	78(9)	-26(8)	-27(8)	25(8)

Table 4. Cation-oxygen distances (pm), calculated with the powder lattice parameters of Y_{0.96}ScO_{2.94} and La_{0.94}ScO_{2.91}.

	Y _{0.96} ScO _{2.94}		La _{0.94} ScO _{2.91}		
Ln: 1	O1	222.2(2)	1	O1	239.9(3)
2	O2	225.9(1)	2	O2	242.3(2)
1	O1	231.3(2)	1	O1	254.2(4)
2	O2	256.8(1)	2	O2	272.3(3)
2	O2	283.5(1)	2	O2	288.0(3)
1	O1	337.7(2)	1	O1	335.0(3)
1	O1	361.8(2)	1	O1	337.9(4)
Sc: 2	O2	207.8(1)	2	O2	209.6(2)
2	O2	209.7(1)	2	O1	210.4(1)
2	O1	211.6(1)	2	O2	211.1(2)

system, Fujifilm, BAS-1800) in order to establish their suitability for intensity data collection. Intensity data were collected at room temperature by the use of a Stoe IPDS-II diffractometer with graphite-monochromatized MoK_α radiation ($\lambda = 71.073$ pm) in oscillation mode. Numerical absorption corrections were applied to the data sets. All relevant crystallographic data and details for the data collections are listed in Table 1.

The atomic parameters of DyScO₃ [28] were taken as starting values of the refinement. Both structures were refined with full-matrix least-squares techniques on *F*² with anisotropic displacement parameters for all atoms (SHELXL-97 [29]). Since the earlier single-crystal studies of REScO₃ (RE = Nd, Sm, Gd, Dy [28], and Eu [30]) revealed defects on the 4*c* RE and the 8*d* oxygen site, the occu-

pancy parameters of all sites were refined in separate series of least-squares cycles. We also observed defects on the 4*c* sites, however, for our crystals both oxygen sites revealed only small defects. The freely refined occupancy values of the 4*c* rare earth (A site) and both oxygen sites approximately accounted for the charge compensation. In the final cycles, the 4*c* rare earth and oxygen occupancies were constrained with the SUMP instruction to ensure correct charge neutrality, leading to the refined compositions Y_{0.96}ScO_{2.94} and La_{0.94}ScO_{2.91} for the investigated single crystals. Final difference Fourier synthesis revealed no significant residual peaks. The positional and anisotropic displacement parameters, and the interatomic distances are listed in Tables 2–4.

Further details of the crystal structure investigation may be obtained from Fachinformationszentrum Karlsruhe, 76344 Eggenstein-Leopoldshafen, Germany (fax: +49-7247-808-666; e-mail: crysdata@fiz-karlsruhe.de, http://www.fiz-informationsdienste.de/en/DB/icsd/depot_anforderung.html) on quoting the deposition number CSD-421747 (Y_{0.96}ScO_{2.94}) and CSD-421748 (La_{0.94}ScO_{2.91}).

NMR spectroscopy

⁸⁹Y magic-angle spinning (MAS) NMR spectra were recorded on a sample doped with 1 mole-% Yb (composition Y_{0.99}Yb_{0.01}ScO₃) at ambient temperature at a frequency of 24.5 MHz on a Bruker DSX-500 spectrometer, using a 7 mm MAS NMR probe operated at a spinning frequency of 5 kHz. 6400 scans were accumulated as rotor-synchronized spin echoes using 90° (180°) pulses of 9 (18) μs length and a relaxation delay of 10 s. The spectrum is referenced to 1 M aqueous YCl₃ solution, using the signal of an 8 M aqueous Y(NO₃)₃ solution containing 0.25 M Fe(NO₃)₃ as a secondary standard. The ⁴⁵Sc magic-angle spinning (MAS) NMR spectra were recorded at ambient temperature at a frequency of 121.63 MHz on a Bruker DSX-500 spectrometer, using a 2.5 mm MAS NMR probe operated at a rotation frequency of 20–25 kHz. Short pulses (0.3 μs, < 20° flip angle) and recycle delays of 0.5 s were used for the acquisition of the spectra, which are referenced against a 0.2 M aqueous solution of Sc(NO₃)₃.

Results and Discussion

Crystal chemistry

The scandates YScO₃ and LaScO₃ crystallize with a strongly orthorhombically distorted GdFeO₃-type structure, space group *Pnma*. Although both compounds have repeatedly been investigated [8–14], herein we report on first single-crystal studies. The structure of LaScO₃ has recently been refined on the basis of powder X-ray diffraction [9], but the present single-crystal data give higher precision for the positional parameters and also allowed a stable refinement of the occupancy parameters. Our investigations complete the series of single-crystal data of rare earth scandates [28, 30, 31] which are excellent substrates for epitaxial growth of perovskite thin films [32].

Due to the large difference in size between La³⁺ (Y³⁺) and Sc³⁺, both cations have distinctly different coordinations. The scandium atoms have almost regular octahedral coordination with small ranges for the Sc–O distances, *i. e.* 208–212 pm for Y_{0.96}ScO_{2.94} and 210–211 pm for La_{0.94}ScO_{2.91}. These octahedra share all corners with adjacent octahedra, leading to the three-dimensional network emphasized in Fig. 1. Due to the strong tilts of the octahedra, the larger yttrium and lanthanum atoms reach 8+4 coordination (Fig. 2). The regular cubooctahedral coordination in the cubic perovskite structure is strongly dis-

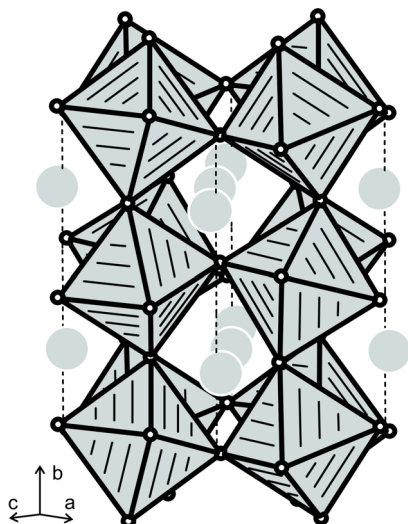


Fig. 1. The crystal structure of LaScO₃. Lanthanum and oxygen atoms are drawn as light-grey and open circles, respectively. The network of corner-sharing ScO_{6/2} octahedra is emphasized.

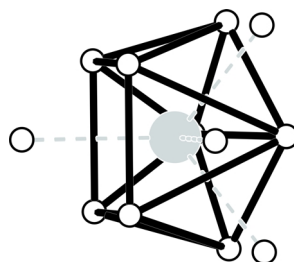


Fig. 2. Coordination of the lanthanum cations in LaScO₃. Lanthanum and oxygen atoms are drawn as light-grey and open circles, respectively. The longer La–O distances are emphasized by dashed lines.

torted. The four longer Y–O and La–O distances are all above 335 pm. A compact and concise overview on the many distortion variants within the family of perovskite-related structures is given in [33, 34].

Finally we need to comment on the composition of the polycrystalline REScO₃ samples and the grown single crystals. So far, small defects on the A sites have only been observed for the Czochralski-grown crystals [28, 32] and now also for flux-grown crystals. The light-yellow color of our flux-grown LaScO₃ sample was a first hint to these defects.

Solid-state NMR spectroscopy

Fig. 3 shows the ⁸⁹Y MAS NMR spectrum of Yb-doped YScO₃. The unique yttrium position is characterized by a single resonance at 265 ppm. This shift lies towards the high end of the range observed for

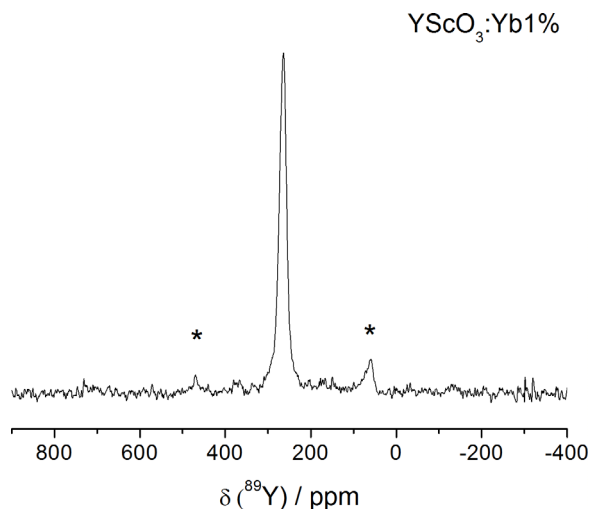


Fig. 3. ⁸⁹Y MAS NMR spectrum of Y_{0.99}Yb_{0.01}ScO₃. Spinning sidebands are indicated by asterisks.

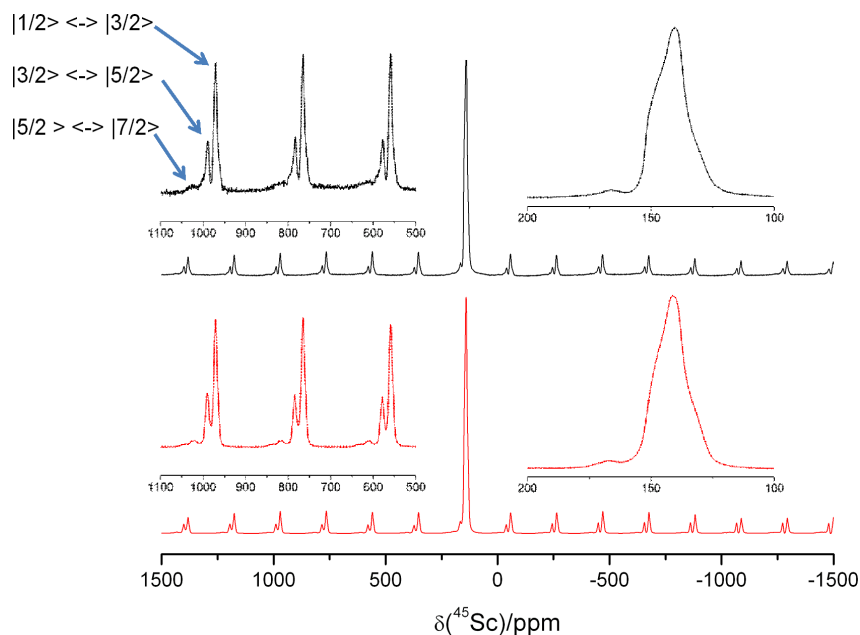


Fig. 4 (color online). ⁴⁵Sc MAS NMR spectrum of YScO₃. The top spectra represent experimental data, the bottom spectra the results of simulations employing the SIMPSON software. The insets on the right show a magnified view of the central transition. The inset on the left shows three sets of spinning sidebands arising from the $|\pm 1/2\rangle \langle -| \pm 3/2\rangle$ and the $|\pm 3/2\rangle \langle -| \pm 5/2\rangle$ and the $|\pm 5/2\rangle \langle -| \pm 7/2\rangle$ Zeeman transitions.

yttrium in oxidic compounds [35–38]. As previously discussed, ⁸⁹Y chemical shifts in oxidic compounds are influenced both by the coordination numbers and the Y–O bond covalencies. As the latter effects seem to be dominated by a simple electrostatic model, considering the Y–O bond ionicity provides a basic qualitative understanding. The Y–O bond ionicity is influenced by the electronegativity of the O-bonded *M* atoms located in the second coordination sphere of yttrium. Strongly electronegative *M* atoms, such as boron and phosphorus, increase the Y–O bond ionicity, resulting in an increased degree of shielding. Conversely, in the case of less electronegative *M* atoms, the Y–O bond covalency is increased, resulting in more positive chemical shift values. The chemical shift of YScO₃ is found in-between those measured for Y₂O₃ (272 and 314 ppm) and YAlO₃ (216 ppm) consistent with the order of the Pauling electronegativities of Y (1.22), Sc (1.36), and Al (1.61) in this series.

The ⁴⁵Sc MAS NMR spectra for LaScO₃ and YScO₃ are shown in Figs. 4 and 5. In these figures, the top spectra represent the experimental data, while the bottom spectra show the results of a full simulation of all the seven Zeeman transitions, which are influenced by first- and second-order quadrupolar perturbations, employing the SIMPSON package and the SPINEVOLUTION programs [39, 40]. For YScO₃ the simulation parameters are $\delta_{\text{iso}} = 153.0$ ppm,

$C_Q = 7.4$ MHz, $\eta_Q = 0.74$. In addition, the spectrum also shows the contributions arising from the six non-central $|m\rangle \langle -| m-1\rangle$ Zeeman transitions. Under static conditions each one of these “satellite transitions” produces an anisotropically broadened powder pattern for polycrystalline samples. Under MAS conditions, however, these powder patterns are converted into three distinct sideband manifolds, corresponding to (1) the $|3/2\rangle \langle -| 1/2\rangle$ and $|-1/2\rangle \langle -| -3/2\rangle$ transitions, (2) the $|5/2\rangle \langle -| 3/2\rangle$ and $|-3/2\rangle \langle -| -5/2\rangle$ transitions, and (3) the $|7/2\rangle \langle -| 5/2\rangle$ and $|-5/2\rangle \langle -| -7/2\rangle$ transitions. As the isotropic second-order quadrupolar shifts affecting these resonances are different from each other [41], three separate spinning sideband manifolds can be observed in these spectra, as shown both in the experimental and simulated data. As theoretically expected [41], the lineshapes of the central $|\pm 1/2\rangle \langle -| \pm 1/2\rangle$ and the outermost $|\pm 7/2\rangle \langle -| \pm 5/2\rangle$ transitions show the strongest second-order quadrupolar broadening effects.

For LaScO₃ the lineshape is influenced by second-order quadrupolar broadening only to a minor extent, and the distinct spinning sideband patterns attributable to the outer Zeeman transitions are strongly overlapped, reflecting distinctly weaker quadrupolar coupling in this case (see Fig. 5). Here, the relevant interaction parameters were extracted by simulating the en-

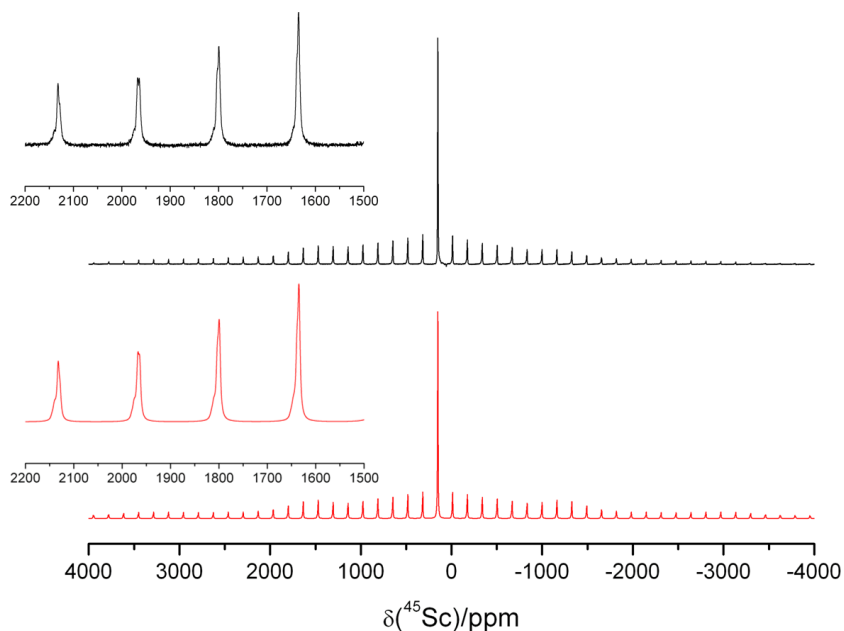


Fig. 5 (color online). ⁴⁵Sc MAS NMR spectrum of LaScO₃. The top spectra represent experimental data, the bottom spectra the results of simulations employing the SIMPSON software. Simulation parameters are $C_Q = 3.4$ MHz and $\eta_Q = 0.8$. The inset shows a magnified view of a part of the sideband manifold. The structure of this lineshape arises from the contributions from the three outer Zeeman transitions.

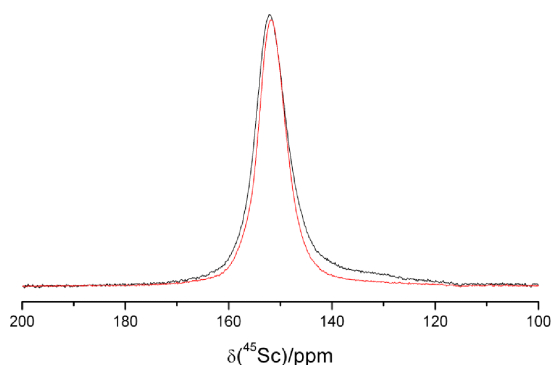


Fig. 6 (color online). ⁴⁵Sc MAS NMR spectra of flux-grown single-crystalline (selected single crystals) LaScO₃ (black) and polycrystalline LaScO₃ (red).

velope of the spinning sideband manifold. We obtained $\delta_{\text{iso}} = 153.5$ ppm, $C_Q = 3.4$ MHz, $\eta_Q = 0.8$.

The ⁴⁵Sc chemical shift values measured for YScO₃ and LaScO₃ are in the typical range of six-coordinate scandium compounds in oxides [18, 19], particularly perovskites [22]. The distinct differences in the quadrupolar coupling constant for ⁴⁵Sc are in qualitative agreement with the larger deviation of the ScO₆ octahedra from ideal octahedral symmetry in YScO₃ (Sc–O bond lengths 208–212 pm; O–Sc–O angles 86.7–93.3°) as compared to LaScO₃ (Sc–O bond lengths 210–211 pm; O–Sc–O angles 88.2–91.8°). The quadrupolar coupling parameters are found in ex-

cellent agreement with the results of a quantum chemical calculation employing the WIEN2k package [42] (see [5] for details of the calculations), producing $C_Q = 8.1$ MHz and $\eta_Q = 0.75$ for YScO₃ and $C_Q = 3.7$ MHz and $\eta_Q = 0.96$ for LaScO₃.

In Fig. 6, the ⁴⁵Sc MAS NMR spectra of polycrystalline LaScO₃ and ground single-crystalline LaScO₃ are compared. The central $|1/2\rangle\langle -1/2|$ transition for the flux-grown single-crystalline sample exhibits a distinctively broader and more asymmetric line shape as compared to the corresponding line shape for the polycrystalline sample, reflecting a distribution of quadrupolar parameters and/or chemical shifts. We note that this observed distribution may be the signature of the deficiency of oxygen in the flux-grown samples. Our attempt to measure a ¹⁹F MAS NMR spectrum (4.65 T; resonance frequency 188.8 MHz, spinning speed 20 kHz, relaxation delays 10–120 s) produced no detectable signal. Based on this result, we consider an exchange of fluorine for oxygen unlikely.

Acknowledgements

This work was financially supported by the Deutsche Forschungsgemeinschaft within SPP 1166. S. B., T. H., and H. D. are indebted to the Alexander von Humboldt Foundation and the NRW Graduate School of Chemistry for research stipends. We are also thankful to Prof. Dr. S. Klemme (Institut für Mineralogie) who let us use his laboratory furnaces.

- [1] G. Adachi, N. Imanaka, *Chem. Rev.* **1998**, *98*, 1479.
- [2] G. Adachi, N. Imanaka, Z. C. Kang, *Binary Rare Earth Oxides*, Springer, Berlin, **2004**.
- [3] S. Geller, *J. Chem. Phys.* **1956**, *24*, 1236.
- [4] C. P. Sebastian, L. Zhang, H. Eckert, R. Pöttgen, *Z. Naturforsch.* **2007**, *62b*, 173.
- [5] C. P. Sebastian, L. Zhang, C. Fehse, R.-D. Hoffmann, H. Eckert, R. Pöttgen, *Inorg. Chem.* **2007**, *46*, 771.
- [6] L. Zhang, C. Fehse, H. Eckert, C. Vogt, R.-D. Hoffmann, R. Pöttgen, *Solid State Sci.* **2007**, *9*, 699.
- [7] T. Harmening, H. Eckert, R. Pöttgen, *Solid State Sci.* **2009**, *11*, 900.
- [8] S. Geller, *Acta Crystallogr.* **1957**, *10*, 243.
- [9] R. P. Liferovich, R. H. Mitchell, *J. Solid State Chem.* **2004**, *177*, 2188.
- [10] Y. S. Savitskaya, M. A. Gurevich, S. V. Kalabukhova, S. I. Sitnikova, *Russ. J. Inorg. Chem.* **1960**, *5*, 1114.
- [11] V. A. Dubok, V. V. Lashneva, N. V. Ul'yanchich, I. G. Donets, I. E. Kir'yakova, *Inorg. Mater.* **1988**, *24*, 391.
- [12] S. Geller, P. Romo, J. P. Remeika, *Z. Kristallogr.* **1967**, *124*, 136.
- [13] J. B. Clark, P. W. Richter, L. Du Toit, *J. Solid State Chem.* **1978**, *23*, 129.
- [14] S. N. Amanyany, V. A. Antonov, P. A. Arsen'ev, K. S. Bagdasarov, D. I. Korolev, D. S. Kholodnyi, *Inorg. Mater.* **1983**, *19*, 855.
- [15] T. Heeg, M. Roeckerath, J. Schubert, W. Zander, Ch. Buchal, H. Y. Chen, C. L. Lia, Y. Jia, C. Adamo, D. G. Schlom, *Appl. Phys. Lett.* **2007**, *90*, 192901.
- [16] T. Bräuniger, K. Ramaswamy, P. K. Madhu, *Chem. Phys. Lett.* **2004**, *383*, 403.
- [17] H. Park, I. Bull, L. Peng, V. G. Young, C. P. Grey, J. B. Parise, *Chem. Mater.* **2004**, *16*, 5350.
- [18] A. J. Rossini, R. W. Schurko, *J. Am. Chem. Soc.* **2006**, *128*, 10391.
- [19] N. Kim, C.-H. Hsieh, J. F. Stebbins, *Chem. Mater.* **2006**, *18*, 3855.
- [20] D. Khabibulin, K. Romanenko, M. Zuev, O. Lapina, *Magn. Res. Chem.* **2007**, *45*, 962.
- [21] C. S. Lue, R. F. Liu, Y. F. Fu, C. Cheng, H. D. Yang, *Phys. Rev. B* **2008**, *77*, 115130.
- [22] D. Mohr, A. S. S. de Camargo, J. F. Schneider, T. B. Queiroz, H. Eckert, E. R. Botero, D. Garcia, J. A. Eiras, *Solid State Sci.* **2008**, *10*, 1401.
- [23] S. Yang, A. A. Popov, C. Chen, L. Dunsch, *J. Phys. Chem. C* **2009**, *113*, 7616.
- [24] N. Kim, J. F. Stebbins, *Chem. Mater.* **2009**, *21*, 309.
- [25] S. Balamurugan, U. Ch. Rodewald, T. Harmening, L. van Wüllen, D. Mohr, H. Eckert, R. Pöttgen, *Z. Naturforsch.* **2010**, *65b*, 13.
- [26] J. P. Remeika, *J. Am. Chem. Soc.* **1956**, *78*, 4259.
- [27] K. Yvon, W. Jeitschko, E. Parthé, *J. Appl. Crystallogr.* **1977**, *10*, 73.
- [28] B. Veličkov, V. Kahlenberg, R. Bertram, M. Bernhagen, *Z. Kristallogr.* **2007**, *222*, 466.
- [29] G. M. Sheldrick, SHELXL-97, Program for the Refinement of Crystal Structures, University of Göttingen, Göttingen (Germany) **1997**. See also: G. M. Sheldrick, *Acta Crystallogr.* **2008**, *A64*, 112.
- [30] V. Kahlenberg, D. Maier, B. Veličkov, *Acta Crystallogr.* **2009**, *E65*, i8.
- [31] T. M. Gesing, R. Uecker, J.-C. Buhl, *Z. Kristallogr. NCS* **2009**, *224*, 365.
- [32] R. Uecker, B. Veličkov, D. Klimm, R. Bertram, M. Bernhagen, M. Rabe, M. Albrecht, R. Fornari, D. G. Schlom, *J. Cryst. Growth* **2008**, *310*, 2649.
- [33] R. H. Mitchell, *Perovskites: Modern and Ancient*, Almaz Press, Thunder Bay, Ontario, **2002**.
- [34] O. Bock, U. Müller, *Acta Crystallogr.* **2002**, *B58*, 594.
- [35] R. Dupree, M. E. Smith, *Chem. Phys. Lett.* **1988**, *148*, 41.
- [36] E. J. Harvey, S. E. Ashbrook, G. R. Lumpkin, S. A. T. Redfern, *J. Mater. Chem.* **2006**, *16*, 4665.
- [37] A. R. Thompson, E. Oldfield, *J. Chem. Soc., Chem. Commun.* **1987**, 27.
- [38] H. Deters, A. S. S. de Camargo, C. N. Santos, C. R. Ferrari, A. C. Hernandez, A. Ibanez, M. T. Rinke, H. Eckert, *J. Phys. Chem. C* **2009**, *113*, 16216.
- [39] M. Bak, J. T. Rasmussen, N. C. Nielsen, *J. Magn. Reson.* **2000**, *147*, 296.
- [40] M. Veshkort, R. G. Griffin, *J. Magn. Reson.* **2006**, *178*, 248.
- [41] D. Freude, J. Haase in *NMR Basic Principles and Progress*, Vol. 29 (Eds.: P. Diehl, E. Fluck, H. Günter, R. Kosfeld, J. Seelig), Springer, Berlin **1993**, pp. 1.
- [42] P. Blaha, K. Schwarz, G. K. H. Madsen, D. Kvasnicka, J. Luitz, WIEN2k, An Augmented Plane Wave Plus Local Orbitals Program for Calculating Crystal Properties, Vienna University of Technology, Vienna (Austria) **2001**.